



Supplement of

Time of emergence of compound events: contribution of univariate and dependence properties

Bastien François and Mathieu Vrac

Correspondence to: B. François (bastien.francois@lscce.ipsl.fr)

The copyright of individual parts of the supplement might differ from the article licence.

S1 Application of the methodology in the Full-ensemble version

In addition to the “Indiv-Ensemble” version, we applied our methodology in the “Full-Ensemble” version, which consists of pooling the contributing variables of the 13 climate models together and applying the methodology to these pooled data to derive a pooled estimate of time of emergence, as well as marginal and dependence contributions. The objectives of the Full-Ensemble version are not the same as those of the Indiv-Ensemble version: whereas the Indiv-Ensemble version permits to analyse the modelling of hazards separately and assess the uncertainty in ToE arising from the inter-model differences, the Full-Ensemble version permits to derive unique ToE estimates and contribution values accounting for the global uncertainty in climate modelling. This Full-Ensemble version assumes that the variables of interest are drawn from the same distribution. Please note that pooling multiple models together may lead to a loss of signal: by assembling the contributing variables together to estimate the CE probability, the pooling procedure can result in mixing the different model signals and noise together. This is particularly true for precipitation and wind changes which are subject to large uncertainties (Shepherd, 2014). However, pooling of model data assumes that each climate model is one valid representation of the physical processes at play in the climate system, and climate simulations being samples from the observed distribution (Srivastava et al., 2021). Thus, even if the climate models have different signals, pooling them and analysing them using our methodology with the Full-version permits to provide useful information on ToE and contribution values by taking into account the complete uncertainty in climate modelling.

Concerning the Full-Ensemble version, a post-processing step of the different models is required for the analysis of compound wind and precipitation extremes only. Indeed, as already explained in Section 2, wind and precipitation data concurrently exceeding high selection thresholds are selected for each climate model in order to focus on compounding extremes. However, climate models can present very different values of wind and precipitation data: for example, a model may not be capable of simulating wind and precipitation events as intense as other models. Hence, each model potentially has different selection thresholds over which values of wind and precipitation are selected. Because of this, selected compound wind and precipitation data from the different climate models cannot be directly pooled, and data need first to be transformed to apply our methodology and analyse pooled extreme events. The transformation step is reached by using a univariate quantile mapping technique (CDF-t, Vrac et al., 2012) that makes the univariate distributions of the wind and precipitation extremes similar to those from a model of reference without modifying their dependence structure. In the following, we choose the CNRM-CM6 model as reference. As values of wind and precipitation extremes of the different models will be modified on purpose by the CDF-t method, note that exceedance thresholds in terms of probabilities (instead of physical values) will be considered. This way, it will enable an interpretation of the results from the Full-Ensemble version. More details about the application of the CDF-t method to transform compound wind and precipitation data for the Full-Ensemble version can be found below.

To analyse growing-period frost events with the Full-Ensemble version, no transformation step is needed before pooling. Indeed, contrary to wind and precipitation extreme, the definition of growing-period frost events does not depend on climate models and can be based on well-established thresholds. As already mentioned, a summary of the successive steps of our methodology for the Full-Ensemble version is displayed in Fig. S1 of the Supplement.

S2 Transformation of wind and precipitation data using CDF-t

As selection thresholds for wind and precipitation extremes are not the same for all the climate models, we need to transform selected wind and precipitation data. For each model, bivariate points of high values are selected using the individual 90th percentiles of wind and precipitation variables. Then, the selected bivariate data from the different models are adjusted with respect to a model taken as reference, using a univariate bias correction technique called the “Cumulative Distribution Function – transform” method (CDF-t, Michelangeli et al., 2009; Vrac et al., 2012). The CDF-t method allows to correct the univariate distribution of a modeled climate variable via a quantile-quantile method that takes into account potential changes of the univariate distribution in the correction procedure. By choosing a model as reference (CNRM-CM6), we use here the CDF-t method to transform marginal properties of selected wind and precipitation values of each climate dataset with respect to CNRM-CM6. This way, marginal distributions of wind and precipitation extremes are similar between the different climate models and are thus more consistent with each other. We consider the 1871-1900 sliding window as reference period for the

calibration of the bias correction. Once data have been transformed for each climate model, bivariate wind and precipitation extreme values from the different models can be pooled and the Full-Ensemble methodology can be applied.

S3 Results for compound wind and precipitation extremes

S3.1 Results for the Full-Ensemble version and a single exceeding threshold

50 We analyse here the results obtained for probabilities of exceeding the 80th percentiles of selected points of high values of wind and precipitation for the 1871-1900 reference period for the Full-version. Fig. S4 presents the results obtained in the same format as those presented in Fig. 7. For the Full-Ensemble version, emergence at the 68% confidence level is detected when considering marginal and dependence changes (Fig. S4a), marginal changes only (Fig. S4b) and dependence changes only (Fig. S4c) of pooled data. Emergence for the Full-Ensemble version can be partly explained by the pooling step which
55 mechanically reduces uncertainties in marginal and copula fitting. Then, confidence intervals, including that of the reference period, are smaller than those obtained for individual models, which leads to emergence of probability signals with small probability changes (as for probability changes induced by dependence changes only in Fig. S4c). Thus, ToE are here detected for the Full-Ensemble version despite the pooling procedure that could reduce the signal by combining models simulating different evolutions of probabilities.

60 Evolution of bivariate FAR, relative differences and contributions time series with respect to the reference period, as well as their decomposition in terms of marginal, dependence and interaction terms are displayed in Figs. S4d, e and f, respectively. Median contributions of marginal, dependence and interaction terms in probability changes are also quantified for the Full-Ensemble version (Fig. S4g). As well as for the Indiv-Ensemble version, Fig. S4g indicates for the Full-version a contribution to probability changes of $\approx 60\%$ from changes in marginal properties and $\approx 40\%$ from changes in dependence properties.

65 S3.2 Results for the Full-Ensemble version and several exceeding threshold

As previously done in Sect. 4.2, we compute times of emergence and contributions for all combinations of exceedance thresholds between the 5th and 95th percentiles, for the Full-Ensemble version in Fig. S10. The results of the Full-Ensemble approach are quite different from those of the Indiv-Ensemble one, i.e., with those of Fig. 8. For example, Fig. S10a indicates that the time of emergence for exceedance probabilities of low wind speed and high precipitation values is ≈ 2000 (while later for Indiv-
70 Ensemble version, i.e. ≈ 2040). The results when considering marginal and dependence changes (Fig. S10a) and marginal changes only (Fig. S10b) are quite similar, indicating that changes in marginal properties mainly drive emergence of probabilities for each of the exceedance thresholds. A clear gradient of ToE values across exceedance thresholds is present: the more extreme the precipitation and the less extreme the wind speed, the sooner the time of emergence of exceedance probability. Conversely, the less extreme the precipitation and the more extreme the wind speed, the later the ToE. In fact, pooling data
75 somehow strengthens the results for time of emergence when models agree on probability changes. Indeed, as seen previously, individual models agree in simulating a significant increase in probability of events exceeding low wind speed and high precipitation values. For ToE induced by dependence properties changes only (Fig. S10c), quite interestingly, probabilities emerge for exceedance thresholds more or less corresponding to the ones identified for Indiv-Ensemble in Fig. 8c. Although dependence properties seem to be stable over time for the majority of the models as observed in Fig. 7c, the resulting dependence structure
80 of pooled data and its changes over sliding windows lead to obtain ToE values of exceeding probabilities. One should also keep in mind that the reduced uncertainty for probability estimations resulting from the pooling process plays an important role in ToE detection for the Full-Ensemble version.

Fig. S10d-f show median contribution of marginal, dependence and interactions terms for the Full-Ensemble version. In particular, the area of exceedance thresholds for which dependence properties contribute greatly to probability changes is greater
85 for the Full-version (Fig. S10e) than for the Indiv-Ensemble version (Fig. 8e). Concerning the interaction term (Fig. S10f), contribution values are equal to 0 for the Full-version.

S4 Results for growing-period frosts for the Full-Ensemble version

Fig. S14 presents the results obtained for the Full-Ensemble version for growing-period frost events. For the Full-Ensemble version, changes of marginal and dependence properties (Fig. S14a) and changes of marginal properties only (Fig. S14b) lead to increase growing-period frosts probability such that time of emergence is detected at 1905 and 1906, respectively. Probability time series are quite similar, suggesting again that changes of dependence properties do not influence strongly probability of growing-period frosts. It is confirmed in Fig. S14c, for which no significant change of probability induced by dependence changes only are observed between the reference and future periods. Median contributions of marginal, dependence and interaction terms in probability changes are reported for Indiv- and Full-Ensemble versions (Fig. S14g). For the Full-
90 version, a dominant contribution of marginal properties to probability changes for growing-period frost events is again obtained.
95

S5 Additional figures

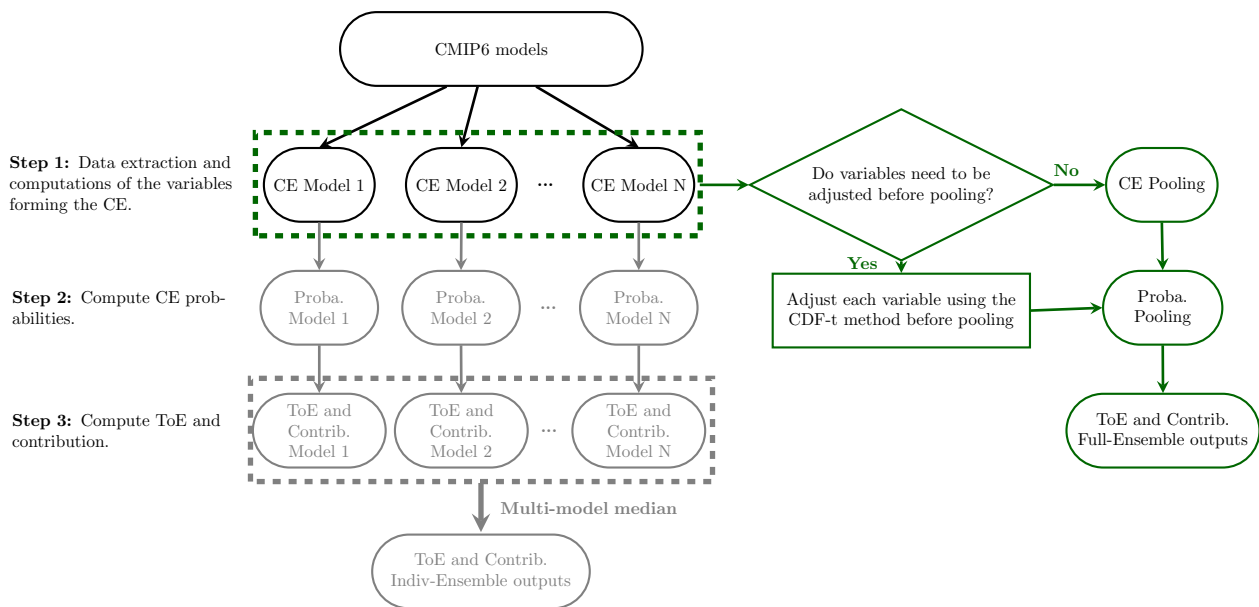


Figure S1. Flowchart for the computations of time of emergence and contributions for Full-Ensemble version. As reminder, the flowchart for the Indiv-Ensemble version is also shown in gray.

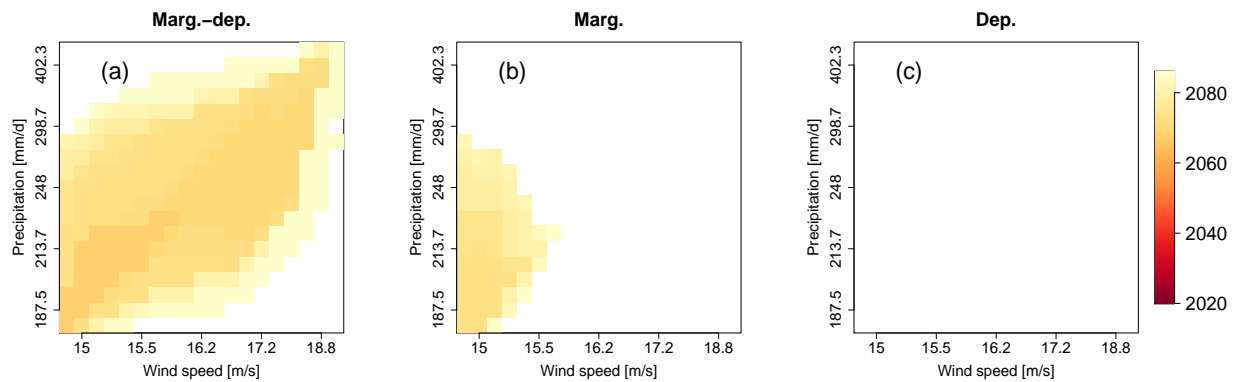


Figure S2. Same as Fig. 6 but for 95% confidence level: CNRM-CM6 (a-c) time of emergence at 95% confidence level for compound wind and precipitation extremes due to changes of (a) both marginal and dependence properties, (b) marginal properties only, and (c) dependence properties only. Results are presented for varying exceedance thresholds between the 5th and 95th percentile of compound wind and precipitation extremes data. White indicates that no time of emergence is detected.

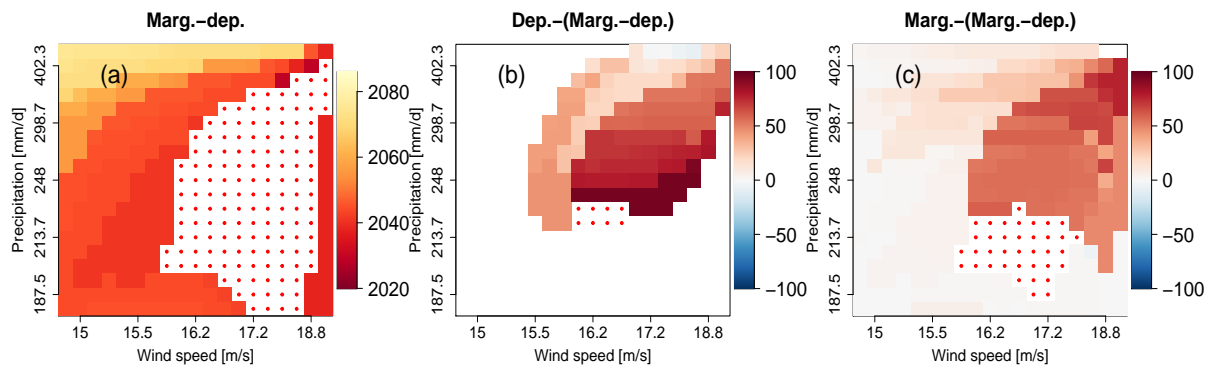


Figure S3. CNRM-CM6 differences of time of emergence at 68 % confidence level between time of emergence obtained by considering both marginal and dependence properties changes and (b) dependence properties changes only, and (c) marginal properties only. CNRM-CM6 (a) time of emergence at 68 % confidence level obtained by considering both marginal and dependence properties changes are also displayed. Color points indicate values lying outside the plotted ranges. White indicates that no time of emergence is detected.

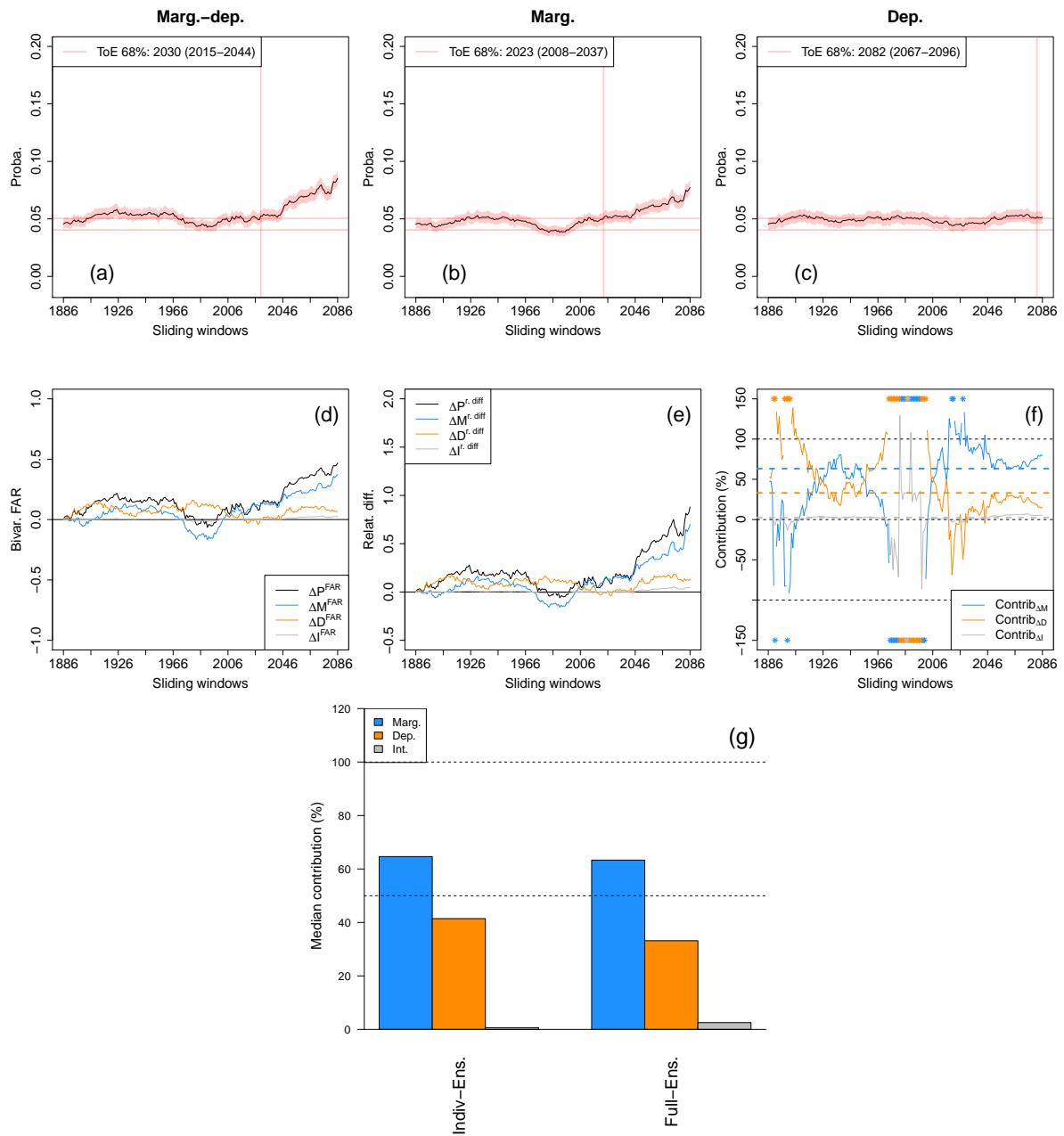


Figure S4. (a-f) Same as Fig. 5a-f but for the Full-Ensemble version. (g) Median contribution of the marginal, dependence and interaction terms to overall probability changes for Indiv- and Full-Ensemble versions.

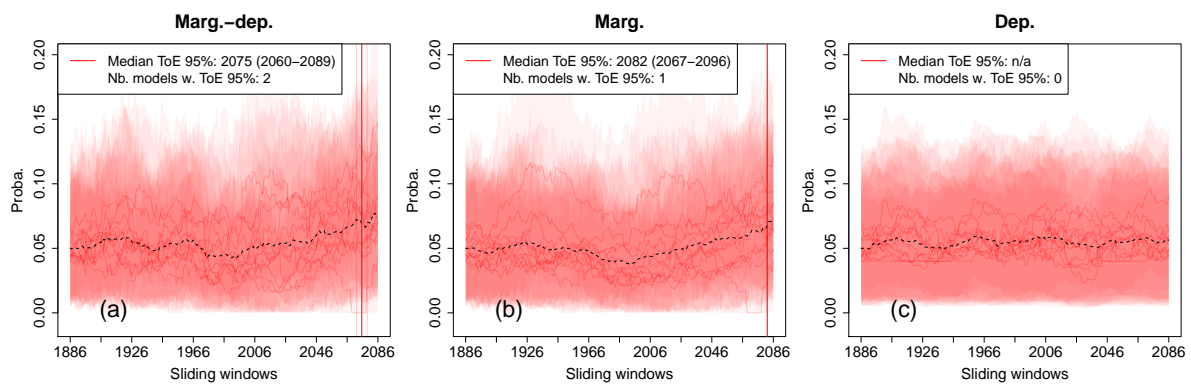


Figure S5. Same as Fig. 7a-c but for 95% confidence level: Probability changes and time of emergence (at 95%) of compound wind and precipitation extremes (exceeding the individual 80th percentiles of selected points of high values) for Indiv-Ensemble version due to changes of (a) both marginal and dependence properties, (b) marginal properties only, and (c) dependence properties only. The shaded bands indicate 95% confidence intervals of the probabilities. Individual time of emergence for the different models within the ensemble are displayed when defined (vertical light red lines), as well as the corresponding median time of emergence (vertical red lines). For information purpose, multi-model mean exceedance probability time series are also plotted (black dotted lines). Not-applicable (n/a) is indicated when no time of emergence is detected.

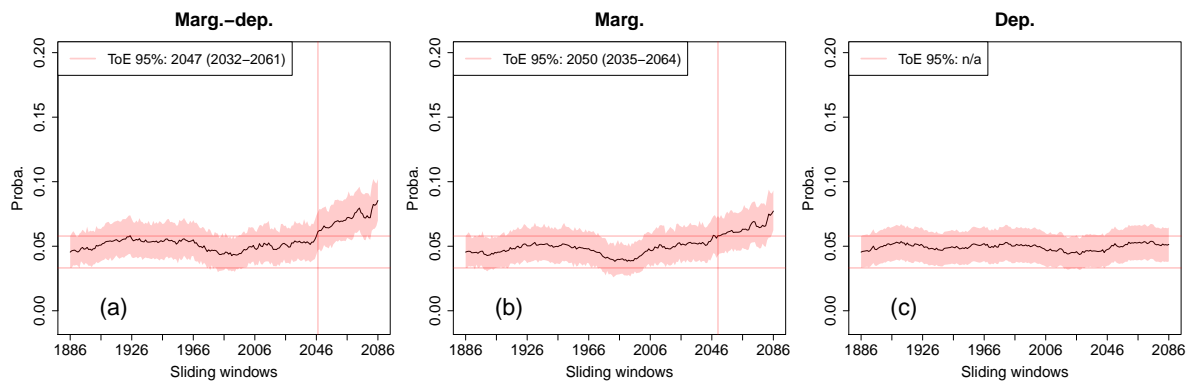


Figure S6. Probability changes and time of emergence (at 95%) of compound wind and precipitation extremes (exceeding the individual 80th percentiles of selected points of high values) for the Full-Ensemble version due to changes of (a) both marginal and dependence properties, (b) marginal properties only, and (c) dependence properties only. The shaded bands indicate 95% confidence intervals of the probabilities. Not-applicable (n/a) is indicated when no time of emergence is detected.

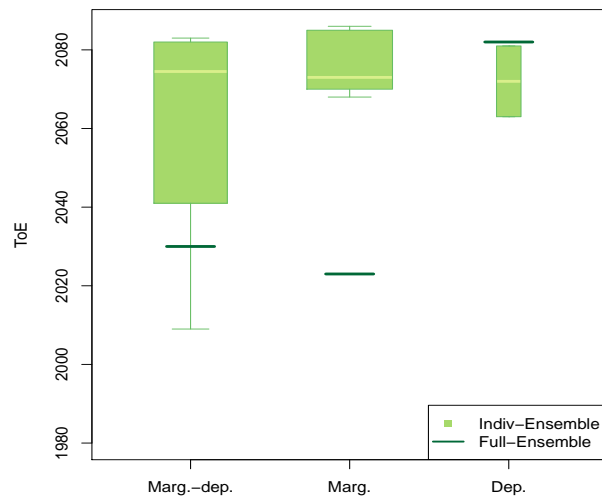


Figure S7. Boxplots of time of emergence at 68% confidence level of compound wind and precipitation extremes (exceeding the individual 80th percentiles of selected points of high values) for the Indiv-Ensemble version. Size of boxplots is proportional to the number of models presenting an emergence. For the Full-Ensemble version, values of ToE are indicated using lines.

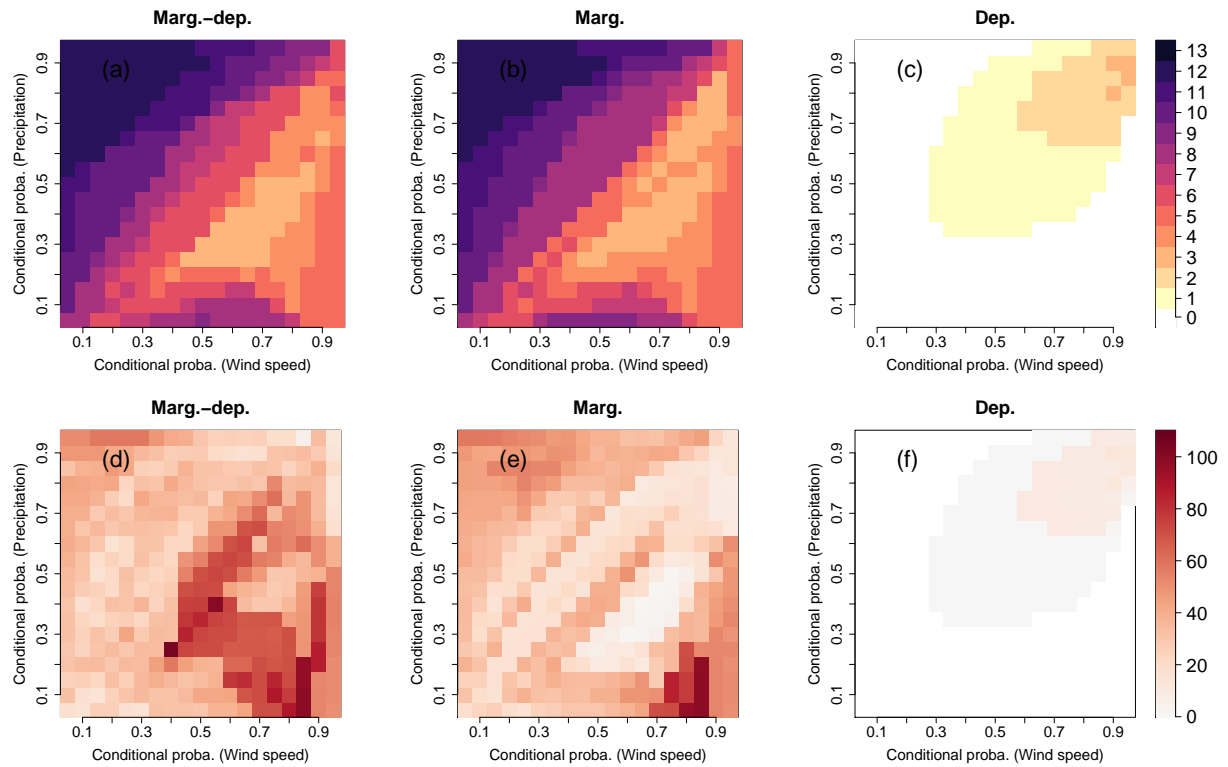


Figure S8. (a-c) Number of models within the Indiv-Ensemble framework presenting a time of emergence at 68% confidence level for compound wind and precipitation extremes. (d-f) Inter-quartile differences (Q3-Q1) of time of emergence.

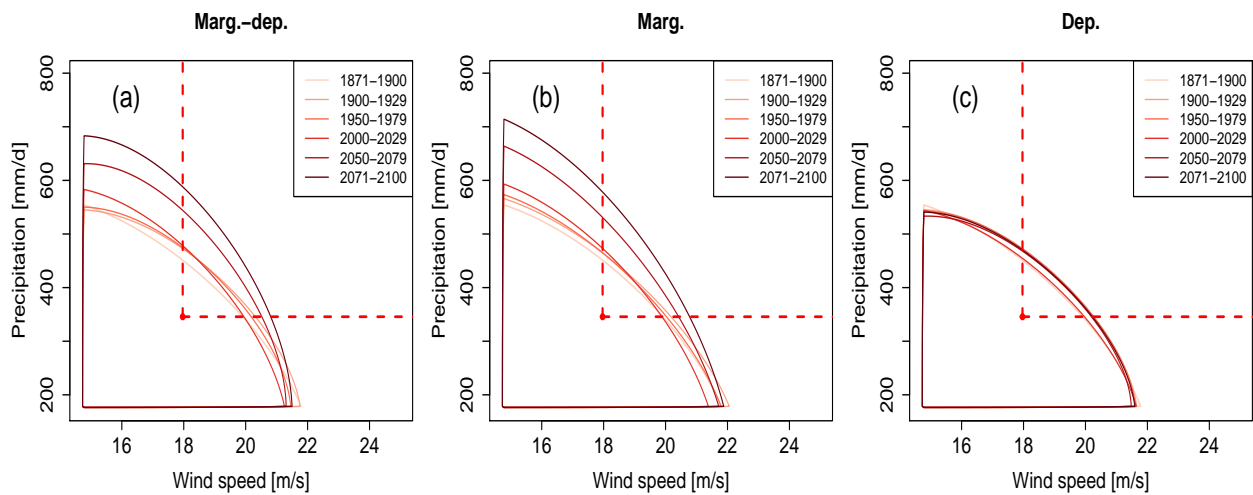


Figure S9. Same as Fig. 4 but for Full-Ensemble data: Change of compound wind and precipitation extremes distributions based on pooled data due to (a) marginal and dependence changes, (b) marginal changes while keeping dependence fixed and (c) dependence changes while keeping marginal fixed. For the bivariate distributions, contour lines encompassing 90 % of all data points are shown. A selection of six 30-years sliding windows is presented using a color gradient from light (1871-1900) to dark (2071-2100).

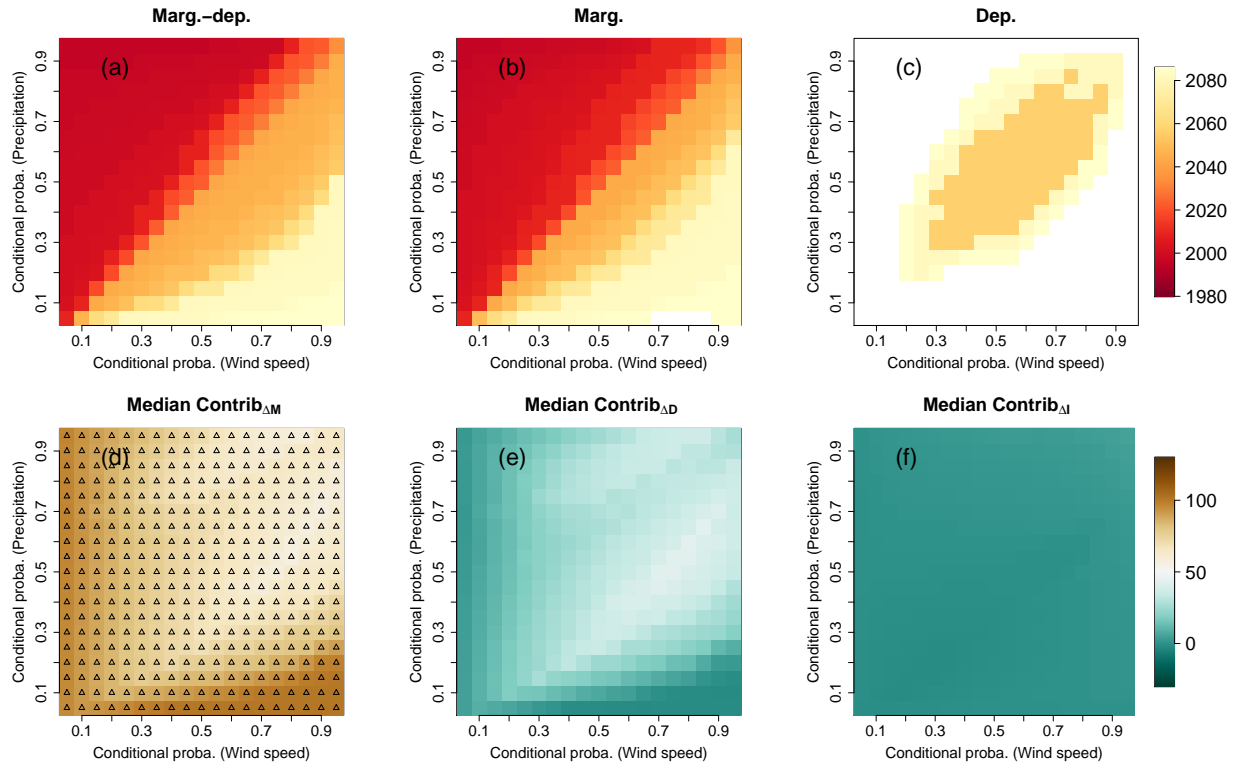


Figure S10. Same as Fig. 8 but for the Full-version: Time of Emergence (at 68% confidence level) matrices of compound wind and precipitation extremes for the Full-Ensemble version due to changes of (a) both marginal and dependence properties, (b) marginal properties only, and (c) dependence properties only. Results are displayed for varying exceedance thresholds between the 5th and 95th percentile of compound wind and precipitation extremes data. For (a-c), white indicates that no time of emergence is detected. Median contributions of (d) marginal, (e) dependence and (f) interaction terms. Upper triangles show where contribution $\geq 50\%$.

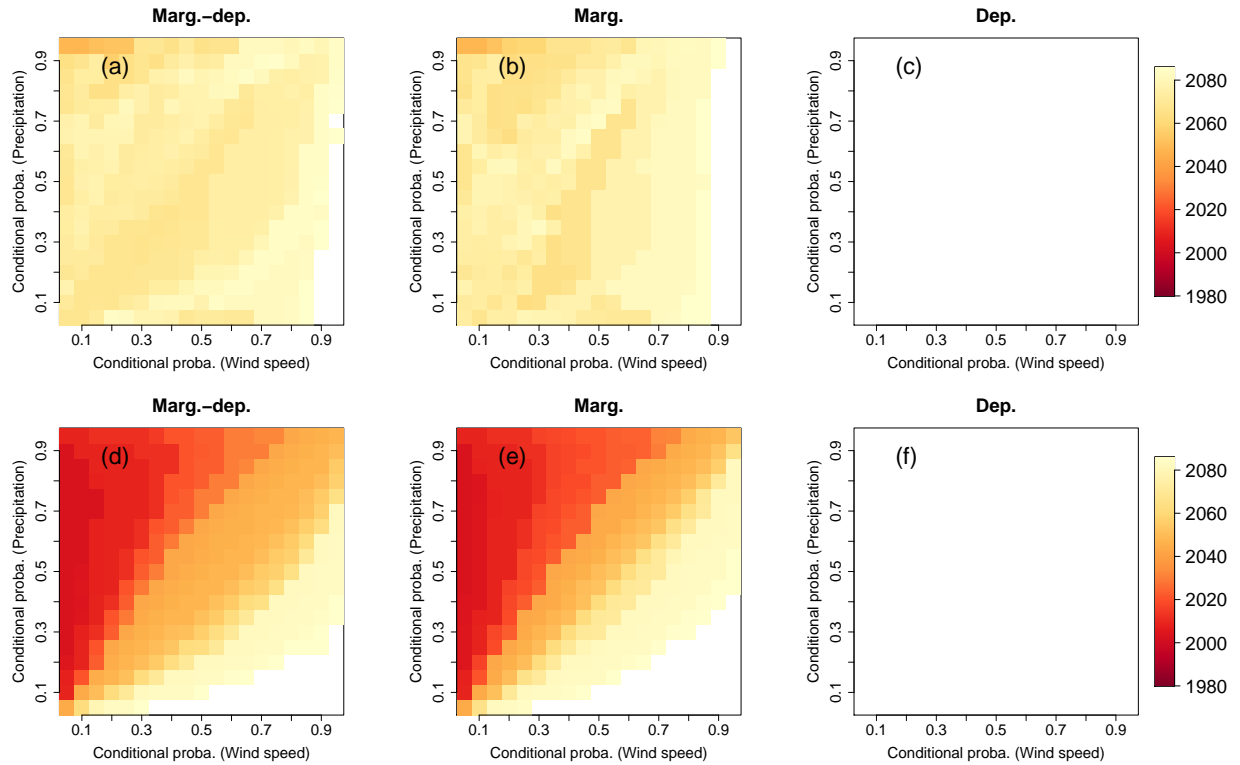


Figure S11. Time of Emergence (at 95% confidence level) matrices of compound wind and precipitation extremes due to changes of (a, d) both marginal and dependence properties, (b, e) marginal properties only, and (c, f) dependence properties only. Results are displayed for (a-c) the Indiv- and (d-f) Full-Ensemble versions for varying exceedance thresholds between the 5th and 95th percentile of compound wind and precipitation extremes data. For each subplot, white indicates that no time of emergence is detected.

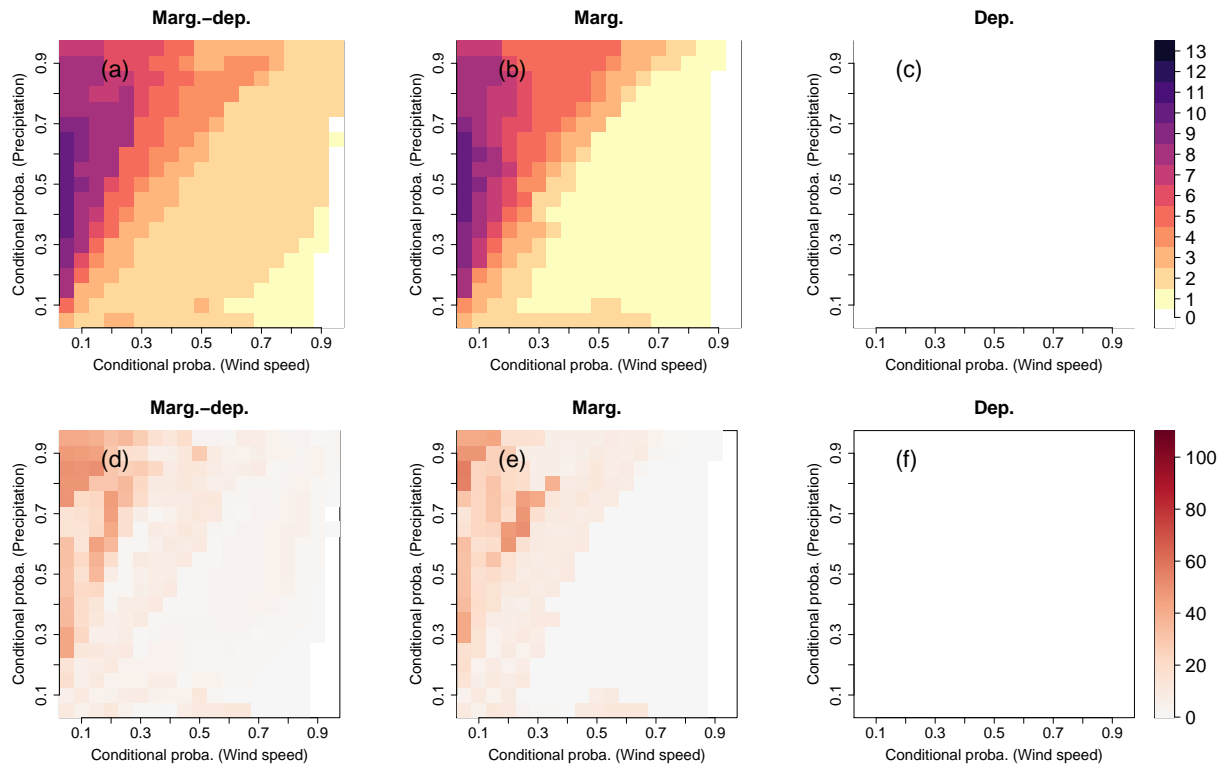


Figure S12. Same as Fig. S8 but for 95% confidence level: (a-c) Number of models within the Individ-Ensemble framework presenting a time of emergence at 95% confidence level for compound wind and precipitation extremes. (d-f) Inter-quartile differences (Q3-Q1) of time of emergence.

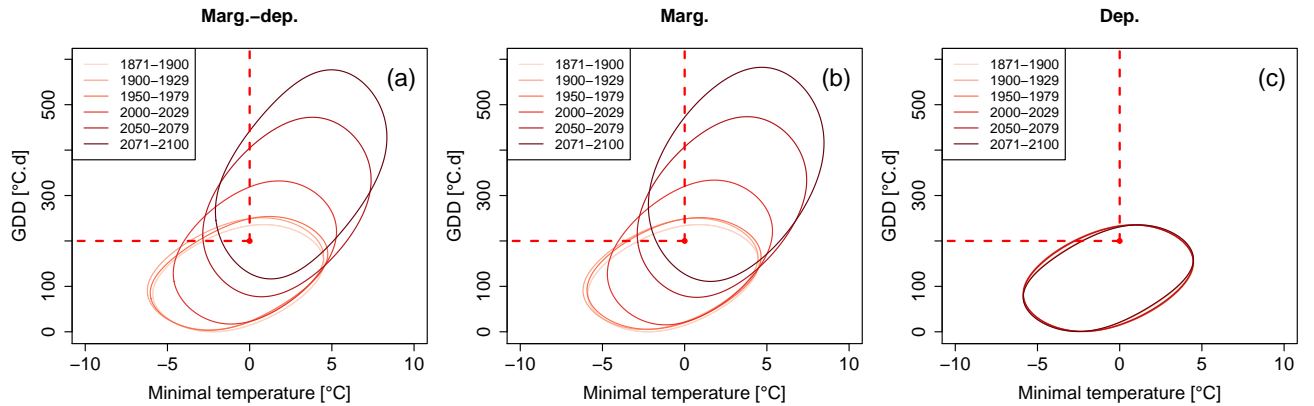


Figure S13. Changes of minimal temperature vs. GDD distributions in Central France for the Full-Ensemble version due to (a) marginal and dependence changes (“Marg.-dep.”), (b) marginal changes while keeping dependence of the reference period (“Marg.”) and (c) dependence changes while keeping marginal of the reference period (“Dep.”). For the bivariate distributions, contour lines encompassing 90% of all data points are shown. A selection of six 30-years sliding windows is presented using a color gradient from light (1871-1900) to dark (2071-2100). A change of bivariate distributions for future periods can be visually assessed when marginal properties changes are considered (panels a and b). The upper-left areas corresponding to probabilities of growing-period frost events ($\{G \geq 200 \cap T \leq 0\}$) are approximately similar for the first sliding windows, but their sizes increase for future periods, suggesting a greater probability of growing-period frosts induced by marginal properties changes. However, when dependence properties changes are only considered without marginal changes (panel c), bivariate distributions are quite similar and the upper-left area is almost identical in size, suggesting that the effect of dependence properties changes on growing-period frost probability is small.

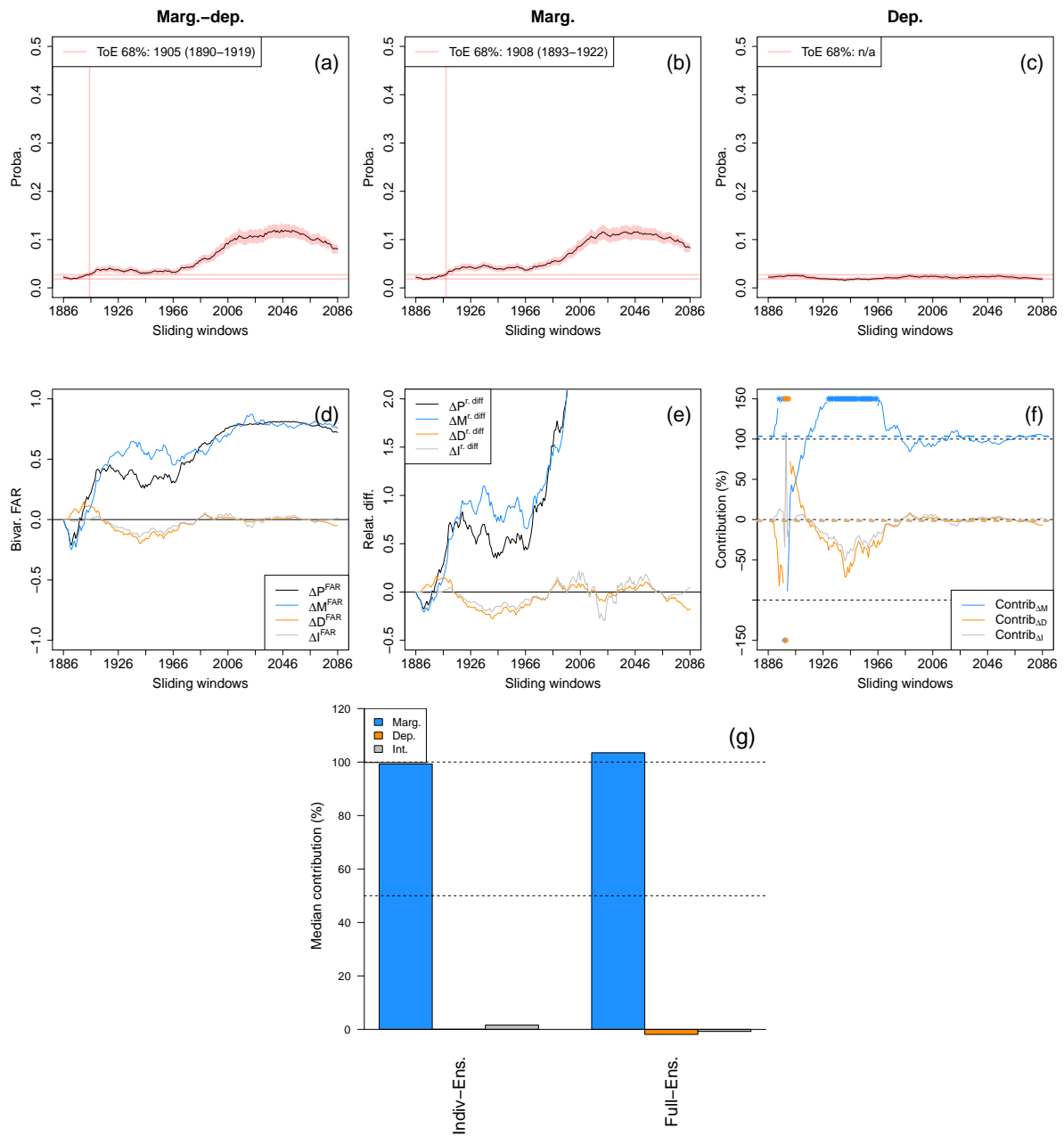


Figure S14. (a-f) Same as Fig. 9a-f but for the Full-Ensemble version. (g) Median contribution of the marginal, dependence and interaction terms to overall probability changes for Indiv- and Full-Ensemble versions.

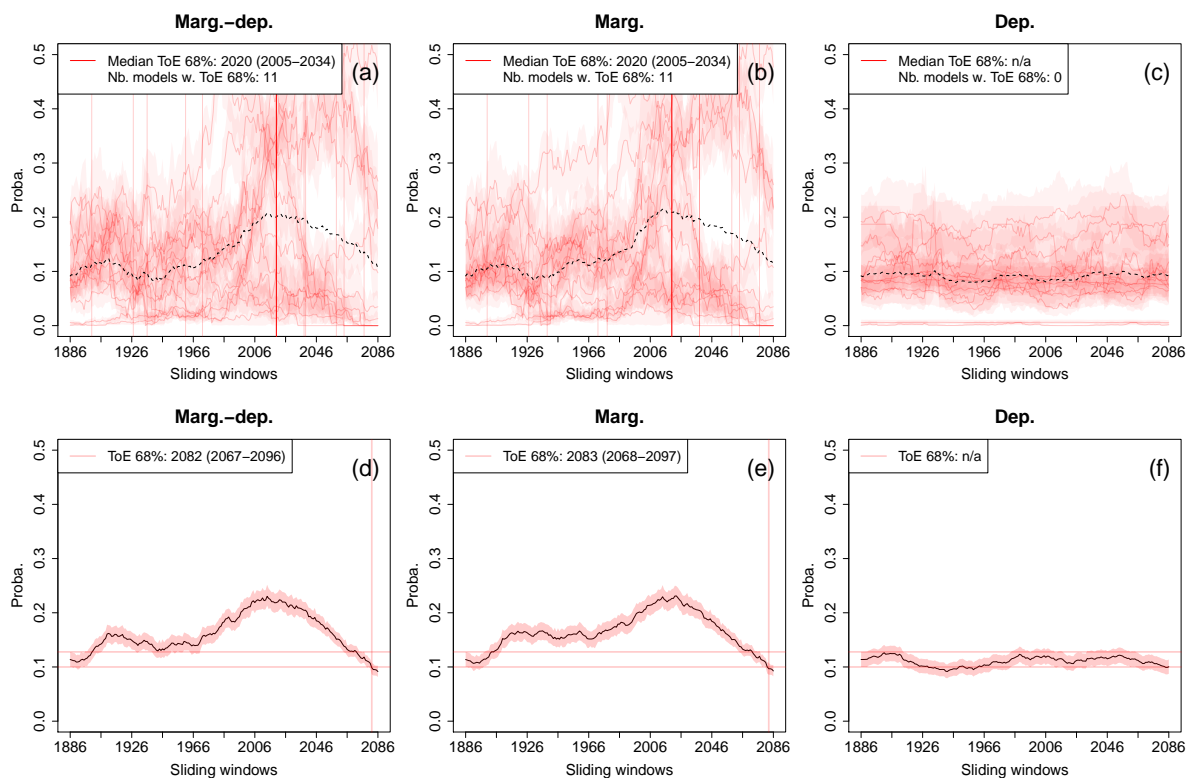


Figure S15. Probability changes and time of emergence (at 68%) of growing-period frosts ($GDD \geq 150$ °C.d and minimal temperatures ≤ 0 °C) for (a-c) Indiv- and (d-f) Full-Ensemble versions due to changes of (a, d) both marginal and dependence properties, (b, e) marginal properties only, and (c, f) dependence properties only. The shaded bands indicate 68% confidence intervals of the probabilities. For (a-c), individual time of emergence for the different models within the ensemble are displayed when defined (vertical light red lines), as well as the corresponding median time of emergence (vertical red line). For information purpose, multi-model mean exceedance probability time series are also plotted (black dotted lines). Not-applicable (n/a) is indicated when no time of emergence is detected.

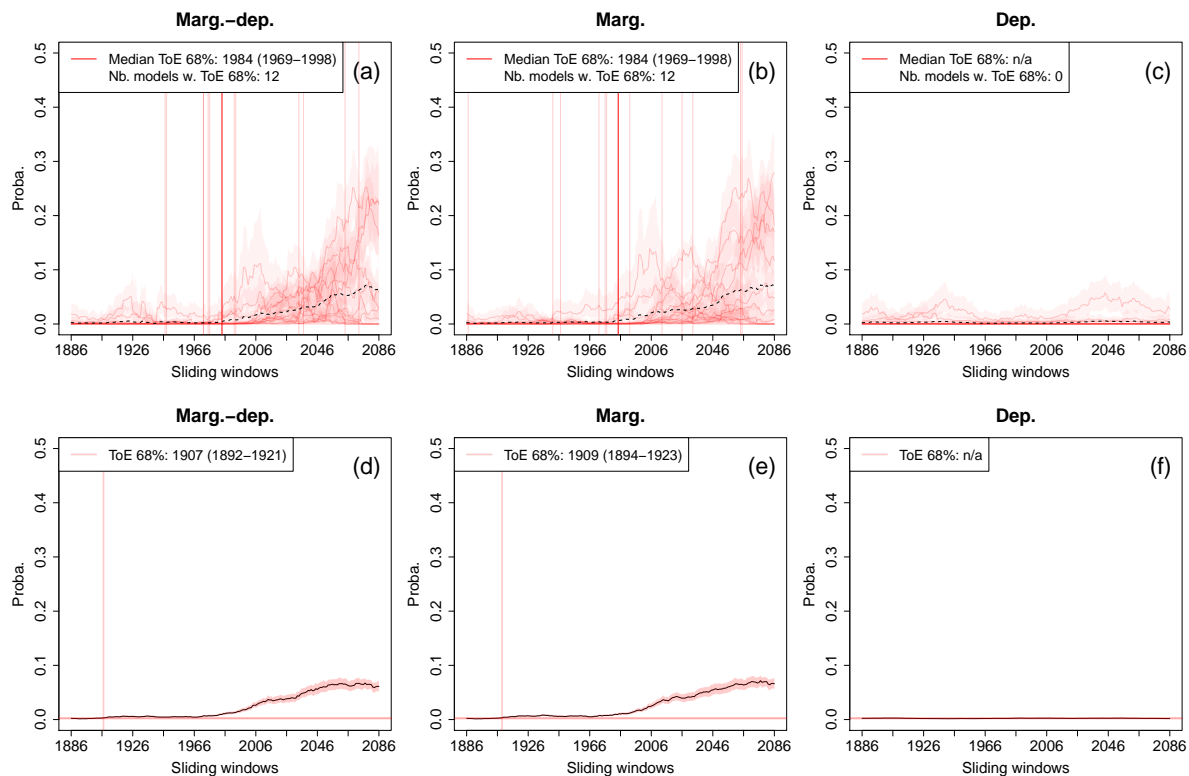


Figure S16. Same as Fig. S15 but for $GDD \geq 250$ °C.d and minimal temperatures ≤ 0 °C: Probability changes and time of emergence (at 68%) of growing-period frosts ($GDD \geq 250$ °C.d and minimal temperatures ≤ 0 °C) for (a-c) Indiv- and (d-f) Full-Ensemble versions due to changes of (a, d) both marginal and dependence properties, (b, e) marginal properties only, and (c, f) dependence properties only. The shaded bands indicate 68% confidence intervals of the probabilities. For (a-c), individual time of emergence for the different models within the ensemble are displayed when defined (vertical light red lines), as well as the corresponding median time of emergence (vertical red line). For information purpose, multi-model mean exceedance probability time series are also plotted (black dotted lines). Not-applicable (n/a) is indicated when no time of emergence is detected.

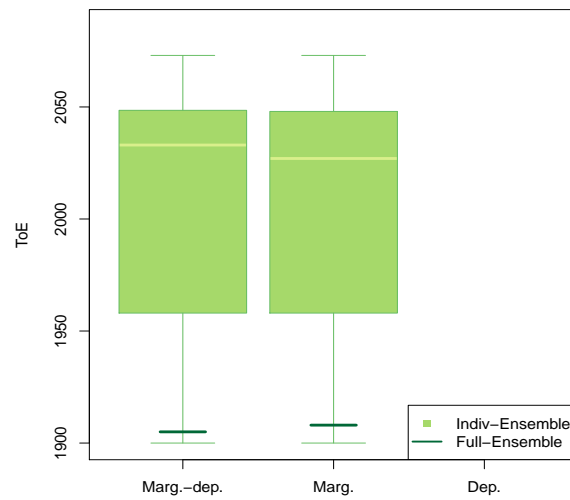


Figure S17. (a) Boxplots of time of emergence at 68% confidence level of growing-period frosts ($GDD \geq 200$ °C.d and minimal temperatures ≤ 0 °C) for the Indiv-Ensemble version. Size of boxplots is proportional to the number of models presenting an emergence. For the Full-Ensemble version, values of ToE are indicated using lines.

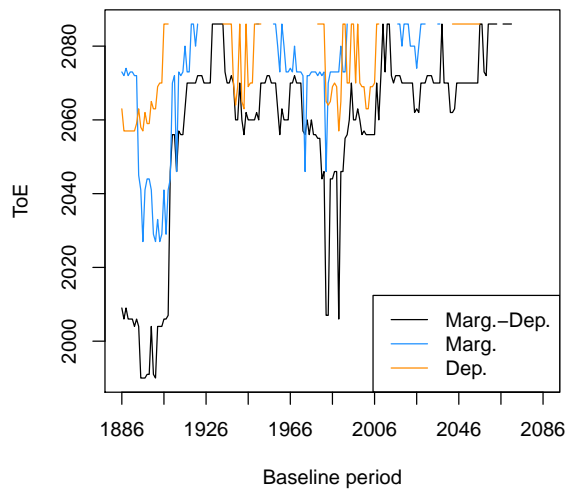


Figure S18. CNRM-CM6 time of emergence (at 68% confidence level) of compound wind and precipitation extremes probabilities ($\mathbb{P}(X > x_{80\text{isel}} \cap Y > y_{80\text{isel}} \mid (X, Y) \in S_{90,90}^{\text{CNRM-CM6}})$) for different baseline periods. Time of emergence are computed for probability time series when considering changes of both marginal and dependence properties (“Marg.-Dep.”), marginal properties only (“Marg.”), and dependence properties only (“Dep.”). A blank space is left when no time of emergence is detected.

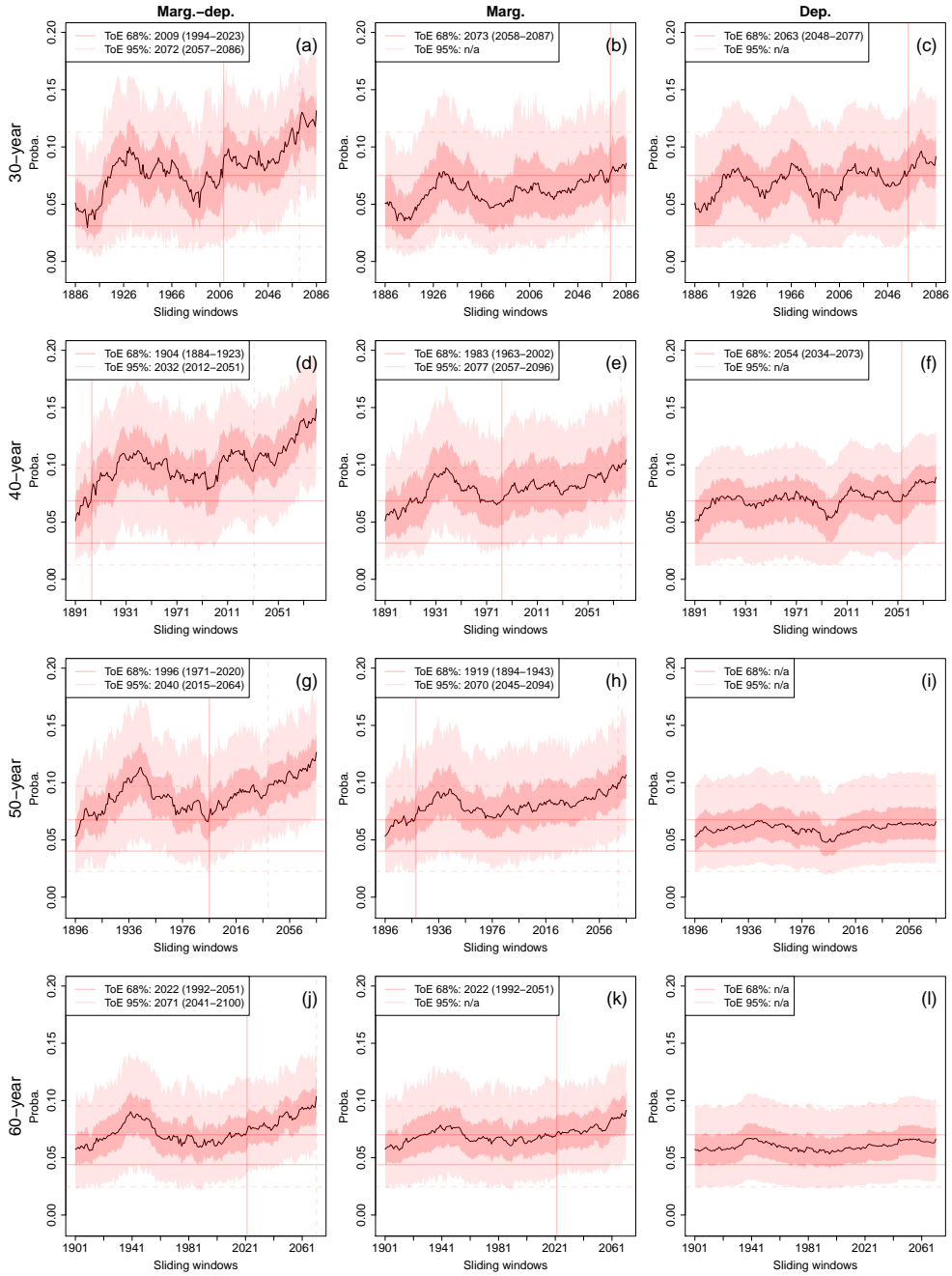


Figure S19. Probability time series and time of emergence of compound wind and precipitation extremes ($\mathbb{P}(X > x_{80\text{sel}} \cap Y > y_{80\text{sel}} \mid (X, Y) \in S_{90,90}^{\text{CNRM-CM6}})$) based on CNRM-CM6 simulations due to changes of (a, d, g, j) both marginal and dependence properties, (b, e, h, k) marginal properties only, and (c, f, i, l) dependence properties only. Results are displayed for probabilities computed by using (a-c) 30-year, (d-f) 40-year, (g-i) 50-year and (j-l) 60-year windows sliding over the period 1871-2100. In each panel, the first sliding window is considered as the baseline period. The shaded bands indicate 68% and 95% confidence intervals of the probabilities. Not-applicable (n/a) is indicated when no time of emergence is detected.

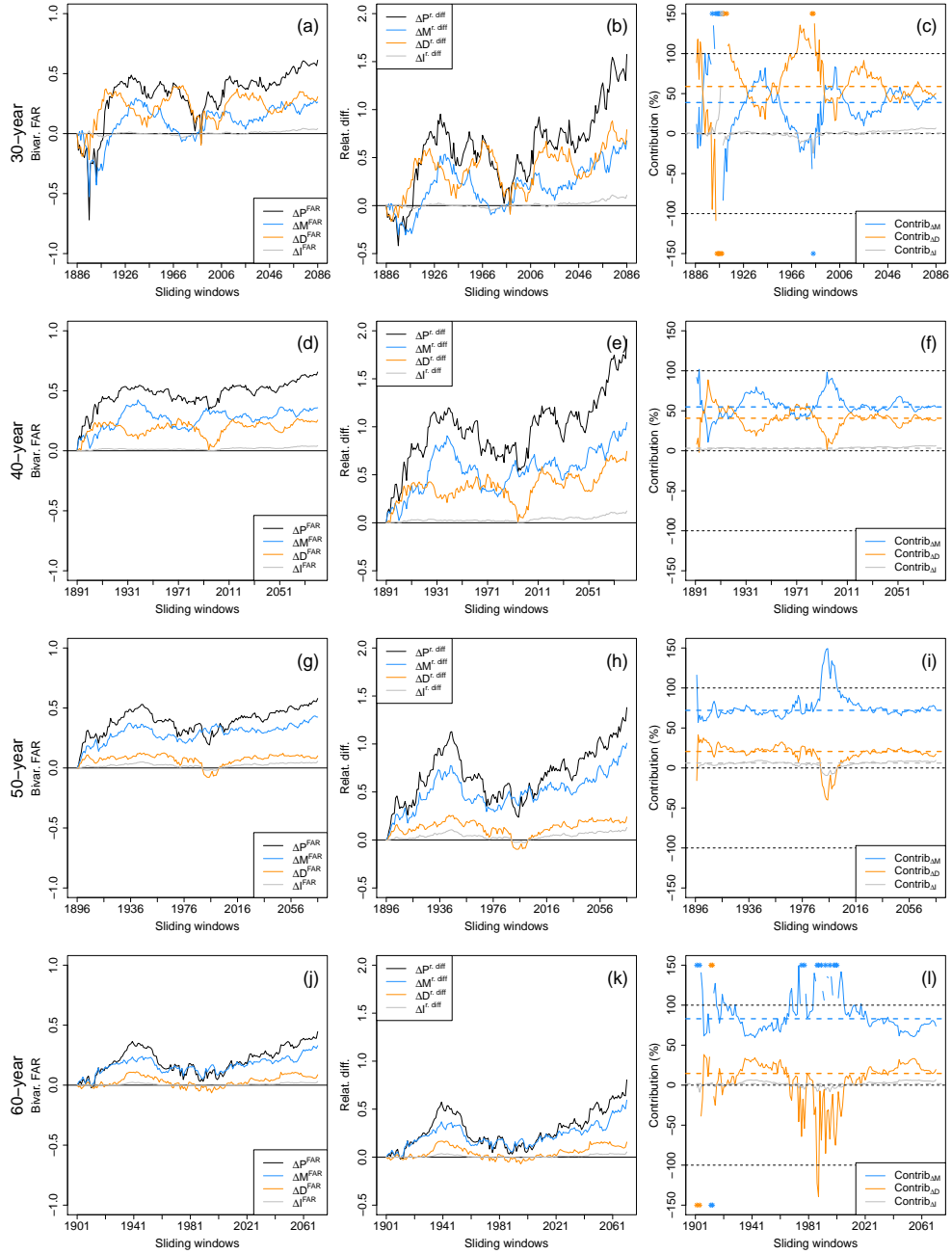


Figure S20. Evolutions of (a, d, g, j) the bivariate fraction of attributable risk (FAR), (b, e, h, k) relative difference of probabilities with respect to the baseline periods and (c, f, i, l) contribution of the marginal, dependence and interaction terms to probability values. Median contributions computed over all sliding windows are displayed with dashed lines. Results are displayed for probabilities computed by using (a-c) 30-year, (d-f) 40-year, (g-i) 50-year and (j-l) 60-year windows sliding over the period 1871-2100. In each application of the methodology, the first sliding window is considered as the baseline period. Asterisks indicate values lying outside the plotted range.

References

- Michelangeli, P.-A., Vrac, M., and Loukos, H.: Probabilistic downscaling approaches: Application to wind cumulative distribution functions, *Geophys. Res. Lett.*, 36, L11 708, <https://doi.org/10.1029/2009GL038401>, 2009.
- 100 Shepherd, T. G.: Atmospheric circulation as a source of uncertainty in climate change projections, *Nat. Geosci.*, 7, 703–708, <https://doi.org/10.1038/ngeo2253>, 2014.
- Srivastava, A. K., Grotjahn, R., Ullrich, P. A., and Sadegh, M.: Pooling Data Improves Multimodel IDF Estimates over Median-Based IDF Estimates: Analysis over the Susquehanna and Florida, *J. Hydrometeorol.*, 22, 971–995, 2021.
- 105 Vrac, M., Drobinski, P., Merlo, A., Herrmann, M., Lavaysse, C., Li, L., and Somot, S.: Dynamical and statistical downscaling of the French Mediterranean climate: uncertainty assessment, *Nat. Hazards Earth Syst. Sci.*, 12, 2769–2784, <https://doi.org/10.5194/nhess-12-2769-2012>, 2012.